CO Adsorption on Monometallic and Bimetallic Au−Pd Nanoparticles Supported on Oxide Thin Films[†]

H. L. Abbott,[||,‡] A. Aumer,[‡] Y. Lei,[‡,§] C. Asokan,[§] R. J. Meyer,[§] M. Sterrer,[‡]
S. Shaikhutdinov,[*,‡] and H.-J. Freund[‡]

Department of Chemical Physics, Fritz Haber Institute of the Max Planck Society, Faradayweg 4-6, Berlin 14195
and Department of Chemical Engineering, University of Illinois at Chicago, Chicago, Illinois 60607

Received: April 28, 2010; Revised Manuscript Received: July 5, 2010

Supported Au−Pd catalysts have been shown to exhibit superior catalytic performances when compared to their monometallic counterparts in a variety of reactions. In addition, the nature of the support often plays a critical role in reactivity. To gain a deeper understanding of the structure−reactivity relationship of the Au−Pd catalysts, here we have employed model systems where monometallic and bimetallic Au−Pd nanoparticles are deposited on well-ordered thin films of reducible and irreducible oxides (i.e., $Fe_3O_4(111)$, MgO(100), and $CeO_2(111)$). Surface structures of the model systems were characterized by temperature-programmed desorption, sum frequency generation, and infrared reflection absorption spectroscopy of CO as a probe molecule. In agreement with previous studies, the results show segregation of gold to the surface. Density functional theory calculations confirm that Au prefers to be at the edges of AuPd alloy particles under vacuum conditions. Strong similarities between the spectral features observed for metal particles on these oxide substrates suggest that the reducibility of the support does not affect the surface structure.

1. Introduction

Highly dispersed gold particles have increasingly gained attention in the catalytic community due to their unusual catalytic properties in a variety of oxidation and hydrogenation reactions (see e.g., refs 1−3 and references therein). The addition of a second metal atom type (e.g., Ag, Cu, Pd, Pt) can have a substantial promotional affect on the catalytic activity as compared to monometallic Au particles.[4−10] Both ligand effects (i.e., an electronic factor due to the change in electron density) and ensemble effects (i.e., a surface structure factor due to the positioning of different atom types) can contribute to the synergistic effects often observed for bimetallic surfaces and particles.[11] In particular, Au−Pd catalysts have been noted for their enhanced reactivity and selectivity in a number of reactions including the direct synthesis of hydrogen peroxide from H_2 and O_2,[8,12] synthesis of vinyl acetate,[13] selective oxidation of alcohols and alkenes,[14,15] CO oxidation,[16,17] and so forth. In addition, support effects were often observed in these systems, in particular catalysts supported on reducible oxides typically showed higher reactivity in oxidation reactions.[18−22]

To gain a clear understanding of the molecular-level reactivity of metal catalysts, model systems composed of metallic nanoparticles deposited on well-defined oxide surfaces have been employed that closely resemble highly dispersed metal catalysts.[23−26] In this paper, we have examined the surface structure of Au−Pd nanoparticles formed on reducible (i.e., CeO_2 and Fe_3O_4) and irreducible (i.e., MgO) metal-oxide thin films. We have used adsorption of CO as a probe molecule since a large database exists in the literature regarding the adsorption of CO on metal surfaces. The observed vibrational frequency of CO adsorbed on the surface can be used to identify its specific binding sites and thus elucidate the surface composition. Desorption of CO as a function of temperature provides similar information and supports the identification of binding sites on the surface. This approach has been successfully applied in the past to investigate Au and Pd particles,[27−30] Au−Pd alloy surfaces,[31] and Au−Pd particles supported on SiO_2[32] and Al_2O_3 films.[33]

2. Methods and Materials

Experiments were performed in two separate ultrahigh vacuum (UHV) chambers with base pressures $\sim 5 \times 10^{-10}$ mbar. Each chamber is equipped with a low-energy electron diffraction/Auger electron spectroscopy (LEED/AES, from Specs) and a differentially pumped quadrupole mass spectrometer (QMS, from Hiden) for temperature-programmed desorption (TPD) experiments. Metal evaporators (EFM3, Omicron) were used for physical vapor deposition of metals. A quartz microbalance was used to determine the deposition rates.

Additionally, one chamber is equipped with infrared reflection absorption spectroscopy (IRAS) using a Bruker IFS 66/vs spectrometer and the other chamber has a Nd:YAG laser system (1064 nm, 30 mJ/pulse, 25 ps, 50 Hz) for sum frequency generation (SFG) spectroscopy. Part of the laser output is converted to 532 and 355 nm light by a harmonic generator. The 1064 and 355 nm beams were mixed in an optical parametric generator/difference frequency generator to produce tunable infrared pulses of about 50−150 μJ/pulse in the range of 3−6 μm with a resolution of $\sim$5 cm^{-1}. The 532 nm light used for SFG had an energy of approximately 200 μJ/pulse. The measured SFG intensities were normalized to the intensities of the incident IR signal.

$CeO_2(111)$ films about 3 nm in thickness were grown by Ce (99.99%, Alfa Aesar) deposition on preoxidized Ru(0001) as previously described in detail.[34−37] The samples showed sharp

diffraction spots in a Ru(0001)-(1.4 × 1.4) LEED pattern characteristic for $CeO_2(111)$ films.

$Fe_3O_4(111)$ films (about 10 nm in thickness) were grown on Pt(111) by repeated cycles of Fe (99.99%, Goodfellow) deposition at 300 K in UHV and subsequent oxidation in 1×10^{-6} mbar of O_2 at 900 K with a final annealing step at 1000 K for 10 min.[38,39]

MgO(100) thin films (about 20 monolayers in thickness) were grown on Ag(100) by deposition of Mg atoms in 10^{-6} mbar O_2 at a sample temperature of 600 K.[40]

The coverage of Au and Pd (both 99.99%, Goodfellow) was determined in situ using a quartz microbalance and has been reported here in a nominal thickness (in angstroms). For preparation of the Au−Pd particles, Pd and Au were codeposited simultaneously. On MgO(100) films, metal particles were deposited at ∼100 K and subsequently annealed at 600 K. On CeO_2 (111) and $Fe_3O_4(111)$ films, particles were deposited at room temperature and annealed to 600 K for 5 min. Subsequently, the particles were stabilized by repeated oxidation−reduction cycles via exposure to 10^{-6} mbar of O_2 at 500 K for 10 min followed by 10^{-6} mbar of CO at 450 K for 10 min. This procedure was used to simulate the calcination-reduction treatment typically used in the preparation of real catalysts and to minimize structural changes during TPD measurements.[29,41]

In CO adsorption experiments, 10 L (1 L = 1 Langmuir = 1×10^{-6} Torr s) of CO were dosed at ∼100 K before spectral acquisition. CO (99.99%, Aldrich) was exposed after passing through a cold trap to remove any volatile impurities such as metal carbonyls.

Density functional theory calculations were performed using the VASP program.[42,43] The calculations utilized a plane wave basis set and ultrasoft pseudopotentials. Exchange and correlation energies were calculated using the PBE functional[44] form of the generalized gradient approximation. Convergence tests were made with respect to the number of k-points and basis set size. A $7 \times 7 \times 1$ k-point grid determined by the Monkhorst-Pack method was employed for the (2 × 2)-Pd(111) surface.[45] A plane wave cutoff energy of 400 eV was used in the calculations. Geometries were judged to be optimized when the forces were within a convergence tolerance of 0.02 eV/Å. Approximately 10 Å of vacuum separated the four-layer slabs in the z-direction.

CO stretching frequencies were calculated by a diagonalization of the Hessian matrix created from the numerical second derivative of the energy with respect to each Cartesian coordinate within the VASP code.

3. Results and Discussion

We first address metal particles deposited onto $CeO_2(111)$ as a support with a well-known surface structure.[34,37] In addition, pristine ceria films do not (or only very weakly) adsorb CO since the $CeO_2(111)$ surface is oxygen terminated. Therefore, all features observed in IRAS and TPD spectra are associated with the metal deposits.

Our previous studies[35–37] using scanning tunneling microscopy (STM) showed that fully oxidized $CeO_2(111)$ films expose atomically flat, wide terraces with a low density of point defects typically attributed to oxygen vacancies. Upon room-temperature deposition, gold first decorates the point defects, then the step edges and the boundaries between rotational domains present on the terraces.[36] Only at coverage above ∼1 Å, Au particles are formed on regular terrace sites as well. An analogous picture was obtained by Zhou et al. for Pd particles,[46] indicating high mobility of Au and Pd adatoms on ceria surfaces. It is therefore
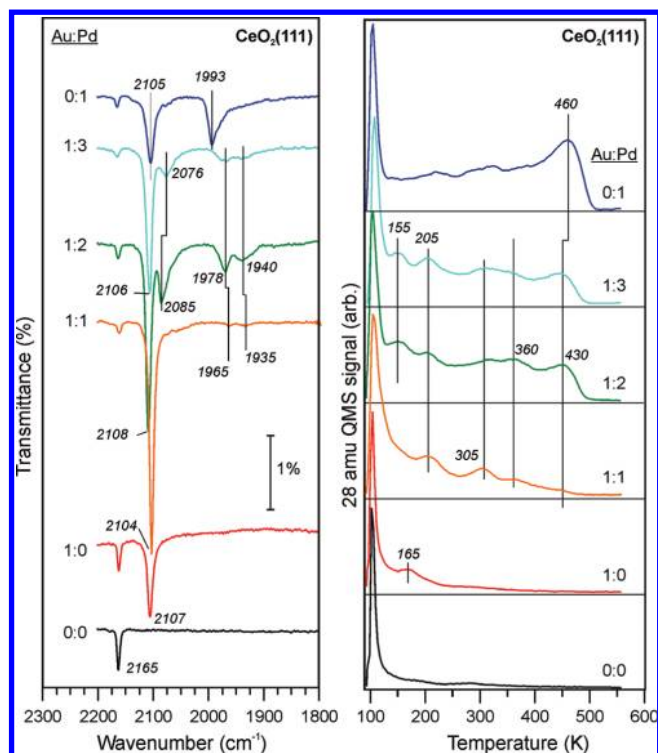

Figure 1. IRAS (left) and TPD (right) spectra for 10 L CO adsorbed at ∼100 K on Pd, Au, and Au−Pd particles supported on $CeO_2(111)$ thin films. The particle composition was varied as indicated by the relative ratios of Au/Pd with a nominal Pd thickness of ∼1 Å. IRA-spectra were acquired at 100 K. Heating rate in TPD spectra is of 5 K/s.

expected that Au and Pd codeposition onto ceria will lead to intermixing of the Au and Pd adatoms, ultimately resulting in Au−Pd bimetallic particles. Annealing to 600 K leads to better intermixing within nanoparticles and also to particles sintering. The CO adsorption results presented below show that separate Au and Pd particles are not being formed. However, there may be a variation in chemical composition of the bimetallic particles.

Figure 1 shows the IRAS and TPD spectra of saturated amounts of CO adsorbed at ∼100 K on metal particles supported by $CeO_2(111)$ films. Bottom spectra show the results for pristine films where the IRAS feature at 2165 cm^{-1}, that is, blue-shifted with respect to CO in the gas phase (2143 cm^{-1}), can be assigned to CO adsorption on Ce^{3+} defect sites or to unsaturated Ce^{4+} sites (see discussion in 47). The fact that the deposition of 2−5 Å of metals (i.e., in amounts sufficient to titrate all point defects[36]) reduces but not totally suppresses this signal, favors its assignment to the line defects such as steps and domain boundaries.

CO weakly adsorbs on Au/ceria particles showing a desorption peak at ∼165 K, in fair agreement with previous data obtained for Au deposited onto FeO(111)[28] and alumina[48] thin films. (The sharp TPD peak at ∼110 K present in all spectra is coming from the heating wires.) The CO molecules chemisorb only on low-coordinated Au surface atoms[49] on atop sites resulting in a single IR band at 2107 cm^{-1}.

For monometallic Pd particles, the CO TPD spectrum is similar to those observed for Pd supported on alumina and silica films,[41,50–53] which are typically rationalized as follows. CO first desorbs from the weakly bound atop sites resulting in a broad plateau-like signal at 100−350 K. As the coverage decreases, the remaining CO molecules occupy energetically more favorable 3-fold hollow sites from which CO desorbs in a well-

CO Adsorption on Au−Pd Nanoparticles

J. Phys. Chem. C, Vol. 114, No. 40, 2010 **17101**

resolved peak at ~460 K. It has been shown[41] that the ratio of these two signals depends on particle size: smaller particles exhibit a larger fraction of terminal CO and hence a larger integral signal at low temperatures. Apparently, this is the case for the Pd/ceria sample studied as shown in Figure 1.

The corresponding IRA- spectrum revealed sharp peaks at 2105 and 1993 cm^{-1}, the latter has a low frequency shoulder overlapping with a broad feature centered at ~1940 cm^{-1}. By comparing to the Pd/alumina system studied in detail in our laboratory,[54] we assign these bands to atop CO species (2105 cm^{-1}); bridge-bonded CO on steps and particle edges (1993 cm^{-1}), and bridge-bonded CO on the (111) facets (1980−1940 cm^{-1}).[32,55] The 3-fold hollow sites on (111) facets exhibiting a band below 1900 cm^{-1} is not observed at this Pd coverage. Certainly, the dipole-coupling effects, in particular at saturated CO coverage, preclude a straightforward quantification of the relative abundance of the corresponding sites. In addition, the metal selection rules[56] applied to IRAS also influence the signal intensity. However, it is apparent that Pd particles formed at ~2 Å coverage are small and expose a high density of low coordinated sites, in agreement with the above TPD results.

As expected, addition of Au to Pd weakens the CO adsorption. It most notably affects the high temperature desorption signal that shifts from 460 to 430 K and ultimately vanishes. Concomitantly, additional desorption features appear at ~155, ~205, ~305, and ~360 K in the spectra and gradually converge to the spectrum for monometallic Au particles.

In the corresponding IRA-spectra. the largest peak at 2105 cm^{-1} gains intensity upon increasing amounts of Au and slightly shifts to 2108 cm^{-1}. A new well-defined peak is observed at 2076 cm^{-1} that blue shifts to 2085 cm^{-1}. The 1993 cm^{-1} peak attenuates while the smaller peaks at 1978 and 1940 cm^{-1} become better resolved. The spectra for the 1:1 ratio and pure gold particles are virtually identical with a single peak dominating the spectra.

Figure 2 shows the IRAS and TPD spectra of CO adsorbed on metal particles supported by Fe$_3$O$_4$(111) films. Bottom spectra show the results for pristine iron oxide films flashed to 800 K prior to metal deposition to prepare a singly terminated surface as judged by STM.[57] The Fe$_3$O$_4$(111) surface is most likely Fe-terminated[38] and therefore adsorbs CO more strongly as compared to the O-terminated CeO$_2$(111) surface. The peak at 2210 cm^{-1} and a broad band centered at 2085 cm^{-1} have previously been assigned to terminal CO adsorbed on Fe^{3+} and Fe^{2+} sites, respectively.[39] The 2210 cm^{-1} band is strongly attenuated upon metal deposition, and the 2085 cm^{-1} band is apparently missing in the presence of, at least, pure Pd and Au particles. The latter suggests that Au(Pd) binds to sites on Fe$_3$O$_4$ that would otherwise be CO adsorption sites. Interestingly, the low-temperature desorption feature characteristic for CO absorbed on a Fe$_3$O$_4$ film (at ~170 K) is still present in the TPD spectra, as more clearly seen in the top spectrum of Pd particles, while the related IRAS features are not. This needs further investigation, and may, for example, be explained by tilted geometry of adsorbed CO, invisible in IRAS due to the metal selection rules.[56]

CO adsorption on Au particles shows a single band at 2110 cm^{-1} that is at a slightly higher frequency than on Au/CeO$_2$. Monometallic Pd particles exhibit pronounced peaks at 2106 cm^{-1} as well as 1991 cm^{-1} and a broad feature at ~1875 cm^{-1}. The latter was not observed for ceria-supported Pd particles, indicating that larger Pd particles form on Fe$_3$O$_4$ as compared to CeO$_2$(111). Indeed, the high-temperature desorption peak at
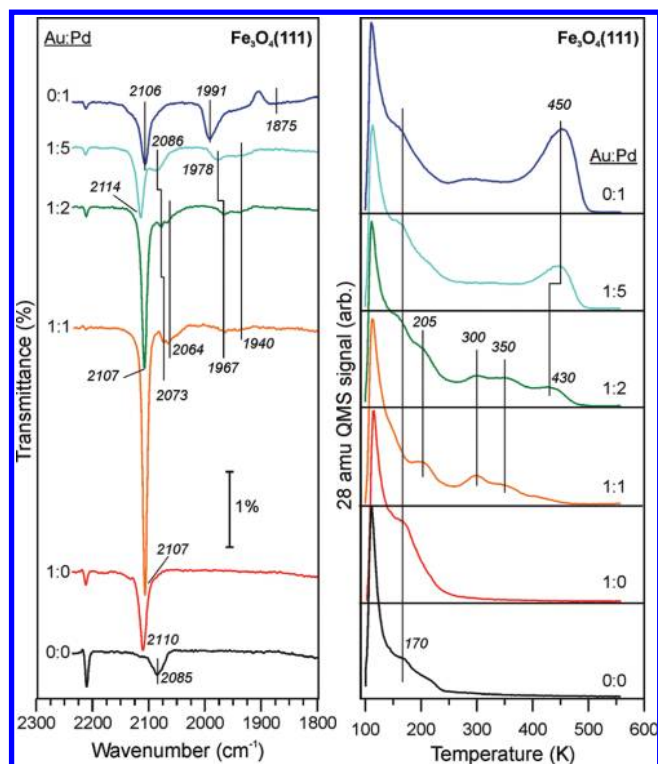

Figure 2. IRAS (left) and TPD (right) spectra for 10 L CO adsorbed at ~100 K on Pd, Au, and Au−Pd particles supported on Fe$_3$O$_4$(111) thin films. The particle composition was varied as indicated by the relative ratios of Au/Pd with a nominal Pd thickness of ~2 Å in monometallic and ~1 Å in bimetallic particles. IRA-spectra were acquired at 100 K. Heating rate in TPD spectra is of 5 K/s.

~450 K characteristic for the presence of (111) facets is more pronounced for Pd/Fe$_3$O$_4$ than Pd/CeO$_2$ at the same Pd coverage.

As in the case of ceria, bimetallic particles show desorption features at 205, 300, and 350 K in addition to the high temperature peak at 450 K that shifts to 430 K and gradually attenuates with increasing amounts of Au. CO desorption at temperatures below 200 K overlaps with desorption from the pristine Fe$_3$O$_4$ film and, as such, these features are undistinguishable in the spectra.

At the lowest Au/Pd ratio (i.e., 1:5) the 2105 cm^{-1} peak shifts to 2114 cm^{-1} and a new band appears at 2086 cm^{-1}. Both signals red shift, that is, to 2107 and 2073 cm^{-1}, respectively, with increasing Au concentration. The sharp band at 1991 cm^{-1} diminishes in intensity, while two peaks become resolved at 1978 and 1940 cm^{-1}. The 3-fold hollow site band at lower frequencies is suppressed in the presence of gold.

Finally, Figure 3 shows the SFG results for CO on Au−Pd particles supported on MgO(100) films. While no signal is observed in the spectra for pure Au particles (most likely due to laser induced heating and desorption of weakly bonded CO), the peaks observed at 2105 and 1991 cm^{-1} for Pd particles agree well with the previous IR spectra for the Pd/Fe$_3$O$_4$ and Pd/CeO$_2$ systems. Small amounts of Au in bimetallic particles (Au/Pd = 1:5) lead to a split in the 2105 cm^{-1} peak observed for Pd alone into the two bands at 2117 and 2093 cm^{-1}, similarly to the case of Au−Pd/Fe$_3$O$_4$ (see Figure 2). In addition, the 1991 cm^{-1} signal disappears leaving a very broad band centered at ~1970 cm^{-1}.

The corresponding CO TPD spectra for Pd/MgO(100) reveal a well-resolved CO desorption peak at 455 K, which shifts to 430 K as Au is added to Pd, and gradually decreases in intensity. The Au-induced desorption features at ~185, ~290, and ~345

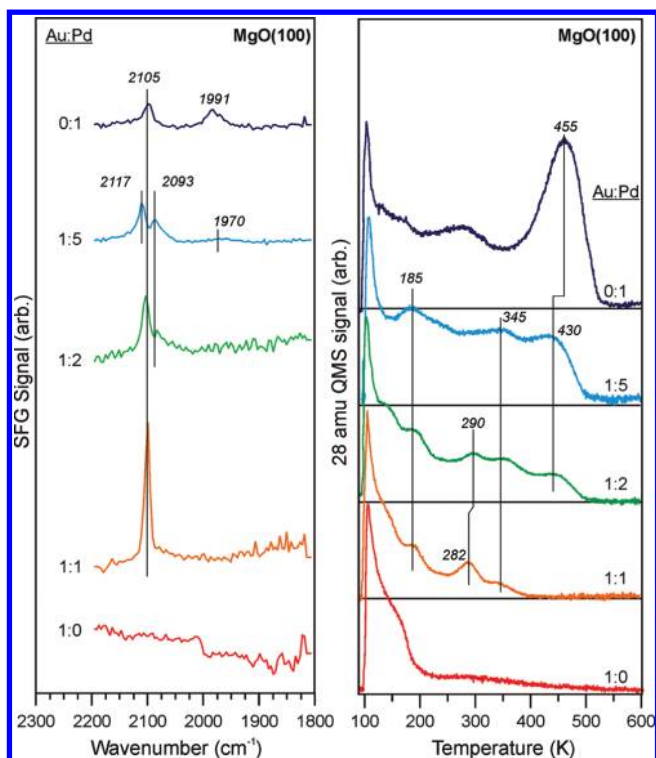**Figure 3.** SFG (left) and TPD (right) spectra for 10 L CO adsorbed at ~100 K on Pd, Au, and Au−Pd particles supported on MgO(100) thin films. The particle composition was varied as indicated by the relative ratios of Au/Pd with a nominal Pd thickness of ~2 Å. The SFG spectra were acquired at 100 K. Heating rate in TPD spectra is of 1 K/s.

K are reminiscent of those observed for Au−Pd bimetallic particles on CeO$_2$ (Figure 1) and Fe$_3$O$_4$ (Figure 2).

Therefore, the results presented in Figures 1−3 show that adsorption characteristics of CO on Pd, Au, and Au−Pd particles supported on Fe$_3$O$_4$(111), MgO(100), and CeO$_2$(111) films are virtually identical for a given coverage. In addition, the spectra are similar to those previously reported for Au−Pd bimetallic particles supported by amorphous films of SiO$_2$[32] and Al$_2$O$_3$.[33] Some deviations may be attributed to the metal coverage (size) effects.

It has previously been shown by STM that monometallic Au and Pd nanoparticles grown on the (111) surfaces of metal oxides primarily expose the (111) facets as having the lowest surface energy and, to a lesser extent, the (100) facets.[48,58] In the first approximation, this must hold true for the annealed bimetallic Au−Pd particles as well. Therefore, tentative peak assignments in IR and TPD spectra of bimetallic particles can be performed on the basis of the results obtained for extended Au−Pd alloy surfaces prepared by annealing of few monolayers of Au deposited onto Pd(111) and Pd(100) single crystals and of their inverted counterparts, that is, Pd on Au(111) and Au(100).[17,31,59−63]

For all supports studied here, bimetallic Au−Pd particles show a similar pattern in the atop region of the vibrational spectra, which consists of a high intensity peak at higher frequency (i.e., 2106−2117 cm^{-1}) and a much lower intensity peak or shoulder at lower frequency (i.e., 2063−2093 cm^{-1}). For extended Au−Pd alloy surfaces, the higher frequency peak, blue shifted with respect to that of pure Pd, is assigned to the CO adsorption on Au, while the lower frequency, red-shifted peak is assigned to Pd atoms surrounded by gold.[32,33]

Addition of Au to Pd most notably affects the IR peak at ~1991 cm^{-1} that vanishes for the smallest amounts of Au

studied here. Since this peak is primarily attributed to bridging CO on Pd particle edge sites,[54,55,64] the results suggest that Au first decorates the edges, ultimately suppressing bonding in bridge geometry and leading to a substantial increase in the intensity of the CO atop species. A similar effect has previously been observed for carbon deposition on alumina-supported Pd particles.[64]

TPD spectra for CO desorption from these three model catalyst systems have three regions corresponding to (i) CO bound on the pristine oxide films and atop to metal atoms in the particles (100−300 K), (ii) CO bound to bridge and edge sites of Pd within the metal particles (300−400 K), and (iii) CO bound to 3-fold hollow sites of Pd within the metal particles (>400 K). Bimetallic particles on Fe$_3$O$_4$, MgO, and CeO$_2$ all show more pronounced peaks in the bridge/edge bound temperature region than were observable for monometallic Pd particles on these films. However, as the concentration of Au in the particles increases, the intensity of the features corresponding to CO desorbing from Pd sites decreases. This behavior is most prominent for the highest-temperature peak (~450 K), which dramatically loses intensity as the gold concentration increases. Thus, the TPD spectra provide compelling evidence that Au preferentially segregates to the surface of bimetallic particles, in good agreement with the previous studies of the Au−Pd alloys.[59,61]

There is no apparent correlation (e.g., "pairing") between the TPD features that would allow us to describe them in terms of CO desorption from different facets constituting the particle surface. Recent combined IRAS and TPD studies of CO adsorption on Au/Pd(111) and Au/Pd(100) surfaces, performed by Tysoe and co-workers, revealed new, Au surface coverage dependent desorption peaks at ~255, 300−335, ~385 K, and ~235, 350−370 K, respectively.[31,61] The lowest temperature features have tentatively been assigned to CO adsorption on Au atop sites that are modified by Pd atoms,[65] and, later, to two CO molecules adsorbed on adjacent atop Pd sites.[31] The desorption in the 300−400 K region, which was accompanied by the disappearance of the IR peak at ~2080 cm^{-1}, has been assigned to CO adsorbed on atop Pd sites as well as on an atop Pd site adjacent to a next-nearest neighbor Pd site, with the remainder of the sites consisting of Au.[31]

Figure 4 shows an IRAS annealing series for 10 L CO adsorbed on the Au−Pd(1:2)/Fe$_3$O$_4$(111) sample illustrating that a similar picture is observed for bimetallic particles. The high-frequency feature (i.e., 2107 cm^{-1}) diminishes in intensity, blue shifts to 2112 cm^{-1}, and disappears upon heating to ~300 K, while the low-frequency feature first gains intensity and then disappears at ~400 K. (Note that CO readsorption may occur while cooling to ~100 K). Basically, similar results were observed by Goodman and co-workers on Au−Pd particles supported on alumina[33] and silica.[32]

In an effort to obtain a more detailed understanding of the results, DFT calculations were performed analyzing both the site preference and frequencies for CO adsorption on Au and Pd surfaces. Both (111) and (221) surfaces were examined.

On Au(111), it is found that coverages of 0.25 ML of CO are not thermodynamically favorable. Only if a larger 3 × 3 cell is used, do we find that CO adsorption can be stabilized at a coverage of 0.11 ML (in the atop position). The coverage of CO is likely underpredicted as the RPBE gives lower adsorption energies than experimental values (just as PW-91 tends to overpredict adsorption energies for CO on metal surfaces[66]). On Pd(111) at 0.11 and 0.25 ML, the hollow site is preferred over bridge and atop sites[67,68] as shown in Table 1. As the
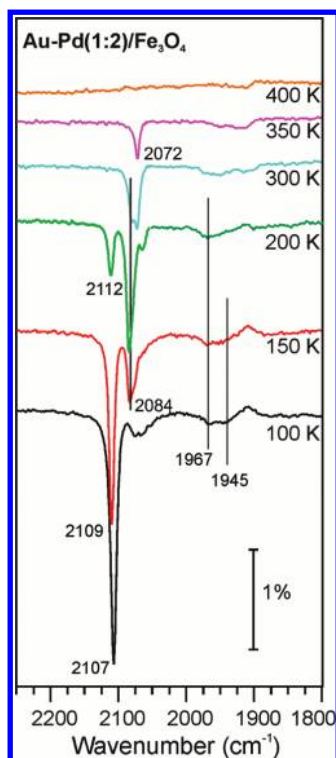
CO Adsorption on Au−Pd Nanoparticles

J. Phys. Chem. C, Vol. 114, No. 40, 2010 **17103**

Figure 4. IRAS annealing series for 10 L of CO adsorbed on Au−Pd (1:2) particles supported on Fe₃O₄(111) thin films. The spectra were acquired at 100 K after flashing to the indicated temperature.

TABLE 1: Calculated Binding Energies and Stretching Frequencies for CO Adsorbed on Different Sites of Au and Pd Surfaces (In All Cases 0.11 ML Coverage of CO)

	Au(111)	Pd(111)	Au(221)	Pd(221)
atop	0.03 eV	−1.18 eV	−0.29 eV	−1.24 eV
	2059 cm⁻¹	2048 cm⁻¹	2054 cm⁻¹	2066 cm⁻¹
bridge	0.15 eV	−1.62 eV	−0.32 eV	−1.64 eV
	1926 cm⁻¹	1868 cm⁻¹	1919 cm⁻¹	1887 cm⁻¹
3-fold hollow	0.18 eV	−1.83 eV	−0.28 eV	−1.69 eV
	1847 cm⁻¹	1802 cm⁻¹	1901 cm⁻¹	1795 cm⁻¹

coverage is increased to 0.5 ML, bridge−atop, bridge−bridge, fcc−hcp, and fcc−atop were all examined. Again, although the fcc−hcp adsorption configuration is favored, the energy differences are not large between these various surface structures (0.3 eV). The gas phase frequency of CO was calculated to be 2103 cm⁻¹, and we therefore apply a scaling factor of 1.02 (from the ratio of 2143/2103) to our frequencies to compare with experimental values. Even when we include this scaling factor, our calculations give vibrational frequencies that are somewhat below those observed in the experiments. (This is at least partially because we have calculated the frequencies in the low-coverage case where dipole−dipole interaction is minimized (and therefore red shifted) and for which the molecules are more strongly bound (and therefore increased back-donation is present also resulting in a red shift of the stretching frequency). However, despite this limitation we can recognize a few obvious trends. First, the CO stretching frequencies do increase as coordination to the surface is reduced. Second, the vibrational frequencies red shift significantly on Pd as compared to Au. On the basis of the capture of simple trends, we hope to gain some insight into the populations of Au and Pd at our surface when CO is adsorbed.

PdAu alloy surfaces of several different varieties were explored. Both Pd-covered PdAu(111) and Au-covered PdAu(111) were
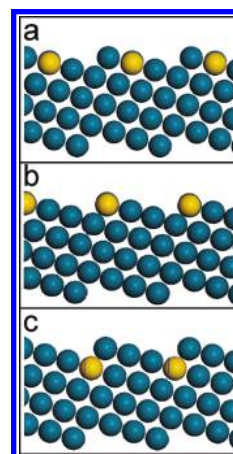

Figure 5. Cross view of the Pd(221) surface, where different locations for the substitution of Au atom (yellow) were examined by DFT.

examined but very little difference was observed between these surfaces and their monometallic counterparts. Second, different configurations of Pd₀.₅Au₀.₅(111) surfaces were explored for a 2 × 2 surface with varying CO coverage from 0.25 to 0.75 ML. It was found that just as in the case for Pd(111), the binding site preference does not agree perfectly with the experimental data as the calculations favor adsorption to more highly coordinated sites than are observed experimentally. However, a key observation is that CO adsorbed on Pd sites on the alloy surface, does red shift slightly as compared to Pd(111) (e.g., Pd bridge shifts to 1815 cm⁻¹) and CO adsorbed on Au sites on the alloy surface does blue shift slightly as compared to Au(111) (e.g., atop shifts to 2104 cm⁻¹) in agreement with previous results.[69] This is likely due to a combination of ligand and strain effects.[11]

Of course, nanoparticles have a large number of edge sites, which may favor less coordinated bonding of CO. Therefore, we have modeled the undercoordinated atoms in our nanoparticles as (221) surfaces as we cannot explicitly calculate the bonding of CO to nanoparticles more than 1 nm in size due to computational cost constraints. We find that on the Pd(221) surfaces, the energy differences between the sites shrink as binding to the atop sites is stronger. Finally, we examined substituted (221) surfaces where one atom of Pd (or Au) is replaced by one atom of Au(or Pd). On Pd(221), three different locations for the substitution of Au were examined, as shown in Figure 5: the terrace (panel a), the top of the step edge (panel b), and the bottom of the step edge (panel c). Au prefers to be located at the edge position by 0.07 eV. Therefore, the results support our experimental observation that Au first modifies CO adsorption on edge sites in alloy nanoparticles. When a single Pd atom is placed in a Au(221) surface, the Pd atom prefers the bottom of the edge by 0.29 eV. However, upon adsorption of CO, the preferred position of Pd switches to the top edge position with a $\Delta E = -0.34$ eV. This implies that small amounts of Pd will gravitate toward the edge positions on small PdAu nanoparticles when CO is exposed to the surface under conditions where migration and restructuring can occur. In our experiments, we do not expose the nanoparticles to CO at elevated temperature and pressure so Pd remains in highly coordinated positions and Au is found in edge positions.

4. Summary

CO adsorption on monometallic and bimetallic Au−Pd nanoparticles deposited onto well-ordered thin films of Fe₃O₄(111), MgO(100), and CeO₂(111) were studied by IRAS (SFG) and TPD

as a function of Au/Pd atomic ratio. In agreement with previous studies, the results show segregation of gold to the surface. DFT calculations confirm that Au prefers to be at the edges of AuPd alloy particles under vacuum conditions. Strong similarities between the spectral features observed for metal particles on these oxide substrates suggest that the reducibility of the support does not affect particle surface structure.

References and Notes

(1) Bond, G. C.; Louis, C.; Thompson, D. T. *Catalysis by Gold*; Imperial College Press: London, 2006.
(2) Haruta, M. *Gold Bull.* **2004**, *37*, 27.
(3) Hutchings, G. J. *Chem. Commun.* **2008**, 1148.
(4) Rojluechai, S.; Chavadej, S.; Schwank, J. W.; Meeyoo, V. *Catal. Commun.,* **2007**, *8*, 57.
(5) Wang, A. Q.; Chang, C. M.; Mou, C. Y. *J. Phys. Chem. B* **2005**, *109*, 18860.
(6) Chimentao, R. J.; Medina, F.; Fierro, J. L. G.; Llorca, J.; et al. *J. Mol. Catal. A: Chem.* **2007**, *274*, 159.
(7) Joshi, A. M.; Delgass, W. N.; Thomson, K. T. *J. Phys. Chem. C* **2007**, *111*, 7384.
(8) Edwards, J. K.; Hutchings, G. J. *Angew. Chem., Int. Ed.* **2008**, *47*, 9192.
(9) Vazquez-Zavala, A.; Garcia-Gomez, M J.; Gomez-Cortes, A. *Appl. Surf. Sci.,* **2000**, *167*, 177.
(10) Schwank, J.; Balakrishnan, K.; Sachdev, A.; Volter, J.; et al. *Stud. Surf. Sci. Catal.* **1993**, *75*, 905.
(11) Gross, A. *Top. Catal.* **2006**, *37*, 29.
(12) Edwards, J. K.; Solsona, B.; Carley, A. F.; Herzing, A. A.; Kiely, C. J.; Hutchings, G. J. *Science* **2009**, *323*, 1037.
(13) Chen, M. S.; Kumar, D.; Yi, C. W.; Goodman, D. W. *Science* **2005**, *310*, 291.
(14) Dimitratos, N.; Lopez-Sanchez, J. A.; Lennon, D.; Porta, F.; et al. *Catal. Lett.* **2006**, *108*, 147.
(15) Enache, D. I.; Edwards, J. K.; Landon, P.; Solsona, B.; et al. *Science* **2006**, *311*, 362.
(16) Piednoir, A.; Languille, M. A.; Piccolo, L.; Valcarcel, A.; et al. *Catal. Lett.* **2007**, *114*, 110.
(17) Gao, F.; Wang, Y. L.; Goodman, D. W. *J. Phys. Chem. C* **2009**, *113*, 14993.
(18) Schubert, M. M.; Hackenberg, S.; van Veen, A. C.; Muhler, M.; Plzak, V.; Behm, R. J. *J. Catal.* **2001**, *197*, 113.
(19) Comotti, M.; Li, W. C.; Spliethoff, B.; Schuth, F. *J. Am. Chem. Soc.* **2006**, *128*, 917.
(20) Edwin, N. N.; Edwards, J. K.; Carley, A. F.; Lopez-Sanchez, J. A.; et al. *Green Chem.* **2008**, *10*, 1162.
(21) Edwards, J. K.; Thomas, A.; Solsona, B. E.; Landon, P.; Carley, A. F.; Hutchings, G. J. *Catal. Today* **2007**, *122*, 397.
(22) Choudhary, V. R.; Samanta, C.; Choudhary, T. V. *Appl. Catal., A* **2006**, *308*, 128.
(23) Campbell, C. T. *Surf. Sci. Rep.* **1997**, *27*, 1.
(24) Henry, C. R. *Surf. Sci. Rep.* **1998**, *31*, 235.
(25) Wallace, W. T.; Min, B. K.; Goodman, D. W. *Top. Catal.* **2005**, *34*, 17.
(26) Libuda, J.; Freund, H.-J. *Surf. Sci. Rep.* **2005**, *57*, 157.
(27) Meyer, R.; Shaikhutdinov, S. K.; Freund, H.-J. *Z. Phys. Chem.* **2004**, *218*, 905.
(28) Lemire, C.; Meyer, R.; Shaikhutdinov, S.; Freund, H.-J. *Surf. Sci.* **2004**, *552*, 27.
(29) Khan, N. A.; Uhl, A.; Shaikhutdinov, S.; Freund, H.-J. *Surf. Sci.* **2006**, *600*, 1849.
(30) Yulikov, M.; Sterrer, M.; Risse, T.; Freund, H.-J. *Surf. Sci.* **2009**, *603*, 1622.
(31) Li, Z.; Gao, F.; Furlong, O.; Tysoe, W. T. *Surf. Sci.* **2010**, *604*, 136.
(32) Luo, K.; Wei, T.; Yi, C. W.; Axnanda, S.; Goodman, D. W. *J. Phys. Chem. B* **2005**, *109*, 23517.
(33) Rainer, D. R.; Xu, C.; Holmblad, P. M.; Goodman, D. W. *J. Vac. Sci. Technol., A* **1997**, *15*, 1653.
(34) Mullins, D. R.; Radulovic, P. V.; Overbury, S. H. *Surf. Sci.* **1999**, *429*, 186.
(35) Lu, J. L.; Gao, H.-J.; Shaikhutdinov, S.; Freund, H.-J. *Surf. Sci.* **2006**, *600*, 5004.
(36) Lu, J. L.; Gao, H.-J.; Shaikhutdinov, S.; Freund, H.-J. *Catal. Lett.* **2007**, *114*, 8.
(37) Baron, M.; Bondarchuk, O.; Stacchiola, D.; Shaikhutdinov, S.; Freund, H.-J. *J. Phys. Chem. C* **2009**, *113*, 6042.
(38) Shaikhutdinov, S.; Ritter, M.; Wang, X. G.; Over, H.; Weiss, W. *Phys. Rev. B* **1999**, *60*, 11062.
(39) Lemire, C.; Meyer, R.; Henrich, V. E.; Shaikhutdinov, S.; Freund, H.-J. *Surf. Sci.* **2004**, *572*, 103.
(40) Sterrer, M.; Risse, T.; Freund, H.-J. *Surf. Sci.* **2005**, *596*, 222.
(41) Shaikhutdinov, S.; Heemeier, M.; Hoffmann, J.; Meusel, I.; et al. *Surf. Sci.* **2002**, *501*, 270.
(42) Kresse, G.; Furthmüller, J. *Comput. Mater. Sci.* **1996**, *6*, 15.
(43) Kresse, G.; Furthmüller, J. *Phys. Rev. B* **1996**, *54*, 11169.
(44) Perdew, J. P.; Burke, K.; Ernzerhof, M. *Phys. Rev. Lett.* **1996**, *77*, 3865.
(45) Hammer, B.; Hansen, L. B.; Norskov, J. K. *Phys. Rev. B* **1999**, *59*, 7413.
(46) Zhou, J.; Baddorf, A. P.; Mullins, D. R.; Overbury, S. H. *J. Phys. Chem. C* **2008**, *112*, 9336.
(47) Binet, C.; Daturi, M.; Lavalley, J. C. *Catal. Today* **1999**, *50*, 207.
(48) Shaikhutdinov, S.; Meyer, R.; Naschitzki, M.; Bäumer, M.; Freund, H.-J. *Catal. Lett.* **2003**, *86*, 211.
(49) Meyer, R.; Lemire, C.; Shaikhutdinov, S.; Freund, H.-J. *Gold Bull.* **2004**, *37*, 72.
(50) Xu, X. P.; Goodman, D. W. *J. Phys. Chem.* **1993**, *97*, 7711.
(51) Xu, X. P.; Szanyi, J.; Xu, Q.; Goodman, D. W. *Catal. Today* **1994**, *21*, 57.
(52) Rainer, D. R.; Vesecky, S. M.; Koranne, M.; Oh, W. S.; Goodman, D. W. *J. Catal.* **1997**, *167*, 234.
(53) Lu, J. L.; Weissenrieder, J.; Kaya, S.; Gao, H. J.; Shaikhutdinov, S.; Freund, H.-J. *Surf. Rev. Lett.* **2007**, *14*, 927.
(54) Wolter, K.; Seiferth, O.; Libuda, J.; Kuhlenbeck, H.; Bäumer, M.; Freund, H.-J. *Surf. Sci.* **1998**, *404*, 428.
(55) Yudanov, I. V.; Sahnoun, R.; Neyman, K. M.; Rosch, N.; et al. *J. Phys. Chem. B* **2003**, *107*, 255.
(56) Hoffmann, F. M. *Surf. Sci. Rep.* **1983**, *3*, 107.
(57) Qin, Z. H.; Lewandowski, M.; Sun, Y. N.; Shaikhutdinov, S.; Freund, H.-J. Unpublished work, 2010.
(58) Hansen, K. H.; Worren, T.; Stempel, S.; Laegsgaard, E.; et al. *Phys. Rev. Lett.* **1999**, *83*, 4120.
(59) Koel, B. E.; Sellidj, A.; Paffett, M. T. *Phys. Rev. B* **1992**, *46*, 7846.
(60) Baddeley, C. J.; Barnes, C. J.; Wander, A.; Ormerod, R. M.; King, D. A.; Lambert, R. M. *Surf. Sci.* **1994**, *314*, 1.
(61) Li, Z. J.; Furlong, O.; Calaza, F.; Burkholder, L.; Poon, H. C.; Saldin, D.; Tysoe, W. T. *Surf. Sci.* **2008**, *602*, 1084.
(62) Han, P.; Axnanda, S.; Lyubinetsky, I.; Goodman, D. W. *J. Am. Chem. Soc.* **2007**, *129*, 14355.
(63) Li, Z.; Calaza, F.; Gao, F.; Tysoe, W. T. *Surf. Sci.* **2007**, *601*, 1351.
(64) Schauermann, S.; Hoffmann, J.; Johanek, V.; Hartmann, J.; Libuda, J.; Freund, H.-J. *Angew. Chem., Int. Ed.* **2002**, *41*, 2532.
(65) Li, Z. J.; Gao, F.; Wang, Y. L.; Calaza, F.; Burkholder, L.; Tysoe, W. T. *Surf. Sci.* **2007**, *601*, 1898.
(66) Mortensen, J. J.; Kaasbjerg, K.; Frederiksen, S. L.; Nørskov, J. K.; Sethna, J. P.; Jacobsen, K. W. *Phys. Rev. Lett.* **2005**, *95*, 216401.
(67) Sautet, P.; Rose, M. K.; Dunphy, J. C.; Behler, S.; Salmeron, M. *Surf. Sci.* **2000**, *453*, 25.
(68) Loffreda, D.; Simon, D.; Sautet, P. *Surf. Sci.* **1999**, *425*, 68.
(69) Yuan, D.; Gong, X.; Wu, R. *Phys. Rev. B* **2007**, *75*, 085428.